IEEE Access
Multidisciplinary | Rapid Review | Open Access Journal

Received December 1, 2020, accepted December 25, 2020, date of publication December 31, 2020, date of current version January 8, 2021.

Digital Object Identifier 10.1109/ACCESS.2020.3048500

Contingency Control Capability of an Optimized HVDC-Based VSC Transmission System

BABATUNDE OLUSEGUN ADEWOLU, (Member, IEEE), AND AKSHAY KUMAR SAHA, (Member, IEEE)
Discipline of Electrical, Electronic and Computer Engineering, University of KwaZulu-Natal, Durban 4041, South Africa
Corresponding author: Babatunde Olusegun Adewolu (adewolubo@gmail.com)

ABSTRACT Power network operations are increasingly becoming complex due to upsurge in power transactions, following the ongoing power system deregulation and restructuring. The alteration in dynamics of power operations based on this upsurge, usually results into contingency because power facilities are made to operate in region of their limits. In this regards, high voltage direct current (HVDC) based voltage source converter (VSC) and other flexible alternating current transmission systems (FACTS) imbedded with VSC have established competence for noticeable diverse power network characteristics improvements. Therefore, this study applies optimized VSC-HVDC transmission system for mitigation of bus voltage and line thermal limit violation as a result of n-1-line outage contingency during bilateral, simultaneous and multilateral transactions. Line contingency evaluation through real power performance index (RPPI) is adopted for severe contingency identification purposes. Optimization of VSC-HVDC system is achieved through statically developed sensitivity-based analysis of VSC control parameters, while its performance for both steady state and contingency conditions are verified with IEEE 6 and 30 bus networks. An improvement in power flow, voltage deviation minimization and automatic alleviation of violated thermal and voltage limits during contingency present optimized VSC-HVDC system as a solution for network performance optimization especially during various transactions occasioned by unbundling power processes. Besides, the superiority of the proposed optimization techniques is established through performance comparison with other sensitivity methods involving reactive power (RPSM), active power (APSM) and performance index (PISM), where the proposed sensitivity method (PSM) outperformed these other methods.

INDEX TERMS Power flow enhancement, VSC-HVDC, sensitivity analysis, n-1 line outage contingency, bilateral, simultaneous, multilateral, power transactions.

NOMENCLATURE

V_{cm}	bus m converter voltage magnitude
θ_{cm}	bus m converter voltage angle
V_{cn}	bus n converter voltage magnitude
θ_{cn}	bus n converter voltage angle
V_m	bus m voltage magnitude
θ_m	bus m voltage angle
Y_{cm}	shunt converter admittance
G_{cm}	shunt converter conductance
B_{cm}	shunt converter susceptance
S_{cm}	bus m injected converter complex power
P_{cm}	bus m injected converter real power
Q_{cm}	bus m injected converter reactive power
I_{cm}	bus m injected converter current
P_m	bus m injected real power
Q_m	bus m injected reactive power
P_{dcm}	bus m converter dc power
P_{dcn}	bus n converter dc power
P_{dcLoss}	dc real power loss
P_{cm}^{spec}	bus m specified control real power
Q_{cm}^{spec}	bus m specified control reactive power
V_n^{spec}	bus n specified control voltage
V_n	bus n voltage magnitude
V_{cm}^{min}	bus m converter lower limit voltage magnitude
V_{cm}^{max}	bus m converter upper limit voltage magnitude
V_{cn}^{min}	bus n converter lower limit voltage magnitude
V_{cn}^{max}	bus n converter upper limit voltage magnitude

The associate editor coordinating the review of this manuscript and approving it for publication was Ali Raza.

G_{mn}	admittance between bus m and n
G_{mm}	bus m total admittance
P_{nm}	active power flow from bus n-m
P_{mn}	active power flow from bus m-n
I_{cn}	bus n injected converter current
I_{cm}^{max}	bus m converter current limit
I_{cn}^{max}	bus n converter current limit
Y_{mn}	line m-n series admittance
θ_{mn}	line m-n series admittance angle
P_{cm}^{cal}	bus m calculated active power
ΔP_{cm}	bus m change in injected real power
ΔP_{cn}	bus n change in injected real power
ΔP^{VSC}	active power mismatch
I_{mn}	current through admittance Y_{mn}
I_m	bus m injected current
I_n	bus n injected current
P_{mn}^{l}	line m-n active power flow limit
w_p	real power weighting factor
N	penalty function
k	bus number
X_{mn}	line m-n reactance
R_{mn}	line m-n resistance
α_{ij}	real loss coefficient
β_{ij}	imaginary loss coefficient
R_{dc}	dc line resistance
θ_n	bus n voltage angle
P_{cm}^{spec}	bus m specified active power

ABBREVIATION

ac	alternating current
dc	direct current
RPPI	real power performance index
VSC	voltage source converter
LCC	line commutated converter
FACTS	flexible alternating current transmission systems
UC	unit commitment
OPF	optimal power flow
NERC	North American Electric Reliability Council
HVDC	high voltage direct current
HVAC	high voltage alternating current
PSO	particle swarm optimization
ABC	artificial bee colony
N-R	Newton Raphson

I. INTRODUCTION

The focus of power network operators to ensure economy of power operation, with utmost consideration for maintenance of system security limits, is facing an accruing challenges because of renewed interest in power industry, consequent of ongoing power network deregulation and restructuring. In order to obtain economic benefits in this regards, utility companies tend to operate network systems in the vicinity of their constraints which could result into congestion issue, affect network security, decrease system reliability and eventually lead to network contingency [1]. To alleviate these problems, system operators can manipulate network topology in favor of reliability and congestion reduction because the solutions to network complexity through generation and transmission expansions are both technically and economically bound [2].

In line with North American Electric Reliability Council (NERC) standard 51, system reliability and security are necessary for operation of power system [3]. This implies that power system planning and operation should be such that an n-1 outage contingency of power components should not disrupt supply to the load. To salvage this situation, several methods which include optimal power flow (OPF), unit commitment (UC), security constrained OPF/UC, redispatch after contingency, reconfiguration of network, contingency management and transmission switching have been in operation, however, some of them are not economically viable [4]–[6].

In the recent time, power electronics devices have made tremendous contributions to the urgency for network capacity enhancement, constrained with sustainability and reliability improvement, with due consideration for minimization of cost, through injection of supplementary controllability and flexibility of operation [7]. The advancement in voltage source converter based technology enables FACTS devices and HVDC systems to play these substantive roles in grid infrastructure sustainability and supports [8]. Among other benefits however, HVDC has been established to be economical for power system transmission over long distance and its application apart from being significant, will determine network grid operation in the future [9]. HVDC surpasses HVAC in asynchronous interconnection of grids, broadened connection of underground cables, minimization of fault currents, mitigation of impacts on environment and network congestion control [10].

The major technology behind the realization of HVDC is via power electronic based semiconductor converters grouped into line commutated converter (LCC) and VSC [11]. Some of the prominent characteristics in favor of VSC-HVDC over LCC-HVDC based systems include but not limited to independent active and reactive power control, black start capability, passive network supply fitness, fast and reliable dynamic performance, stability of ac operation, compact station structure, flexibility of operation among others [12], [13]. Increase in application of VSC-HVDC will increase the integration of more renewable generations, expand bidirectional flow of ac grid current, expand efficiency of grid transmission, enhance distributed generation connections and improve system security as well as reliability which will eventually redirect forthcoming grid operations and redefine future grid architectures [14], [15].

Steady state model of VSC-HVDC system feeding ac grid was presented in [16] for the purpose of derivation of active and reactive power flow constraints satisfaction. Fault current protection capability of VSC-HVDC interconnecting wind farm and ac grid was demonstrated in [17]. It was concluded here that traditional protection systems were

impacted as a result of manipulation of both magnitude and phase angle of fault current by the presence of VSC-HVDC transmission system. Deployment of VSC-HVDC network interconnection for frequency support service provision was studied using temperature dependent overload capability in [18], while small signal stability investigation conducted through controlled OPF in [19] revealed that, an ac network embedded with VSC-HVDC system is more stable. With focus on maintaining transmission equilibrium and stability of the grid, an OPF approach based on minimum power loss was developed for a multiterminal VSC-HVDC grid [20].

Assessment of stability performance of an embedded VSC-HVDC transmission system through interactive dynamic behavior was investigated with inference of an improved system dynamic performance [21]. In order to improve dynamic performance and enhance system stability however, artificial bee colony (ABC) was engaged for optimal scheduling of VSC-HVDC gain in the work presented by Ramadan *et. al* [22]. In a similar work, the control parameters of VSC were tuned using particle swarm optimization algorithm (PSO) for steady state and dynamic performance enhancement of VSC-HVDC system [23]. Wang *et al.*, studied the effects of dissimilar reactive power control strategies on transient and dynamic stability of an ac system, with conclusion that oscillation control and voltage sustenance were influenced especially at the instance of grid disturbance [24]. It was concluded in [25] however, that VSC-HVDC have an impact on interdependency of power system dynamics and that further studies are required to fully understand their impact on system stability improvement and ancillary support services.

The technology of VSC-HVDC system is fast evolving, with entrenched countless potentials and its suitability in terms of transient stability, dynamic stability and oscillation damping have received increasingly great research attentions. However, wide range of ac network support benefits, and other ancillary services formed bulk of renewed research focus for deployment and application of VSC-HVDC systems. Therefore, this study investigates power network contingency control capability of an ac network embedded HVDC based VSC transmission system. The optimization of VSC-HVDC system location was achieved through sensitivity-based approach with consideration for inclusion of HVDC line loss in the system total loss. This sensitivity based optimally placed HVDC system is therefore offered as a solution to challenges of contingency mitigation in network systems. The provision of ancillary support service which include system limits violation restoration at the instance of an n-1 line outage contingency is well investigated and analyzed. The need for increase in network transmission potentials to accommodate diverse nature of power transactions occasioned by power sector liberalization forms the motivation for this research work. The following are the contributions of this study;

1. Optimization of VSC-HVDC transmission system based on sensitivity approach for ac network incorporation.
2. Investigation of power flow improvement and bus voltage profile deviation minimization of ac network embedded with VSC-HVDC transmission system.
3. Investigation of VSC-HVDC transmission system ancillary support services during contingency. The following are the major steps taken to achieve the listed objectives;
    a) Modelling of an ac embedded VSC-HVDC line using lumped π-equivalent parameters representation for HVDC line loss determination.
    b) Application of mathematical equations of total system loss involving HVDC line loss for derivation of sensitivity-based solution for optimal placement.
    c) Presentation and ranking of resultant sensitivity for voltage magnitude control and control angle of VSC-HVDC transmission system for optimization.
    d) Performance of load flow of an ac network with alteration in Jacobean elements.
    e) Ranking and selection of the most severe n-1 line outage contingency.
    f) Implementation of load flow with n-1 line outage contingency.
4. Unlike other sensitivity-based approaches, the impacts of the loss especially of the line containing the device on the optimization process is a unique hallmark of this approach and hence, performance comparison of the proposed placement approach with other sensitivity methods is carried out.

The remaining part of the paper is arranged in the following manner: Description of VSC-HVDC system is contained in Section 2. VSC-HVDC Sensitivity based optimal placement approach is highlighted in Section 3. Results are presented and discussed in Section 4. Findings and outcome of the research are concluded in Section 5.

II. VSC-HVDC SYSTEM

VSC-HVDC system is made up of two VSCs, which are interconnected with dc conductor for the purpose of this study. At every point however, one VSC operates as a rectifier while the other acts as an inverter for purposeful transmission of highly controlled and constant power between themselves [26]. Each converter can control either voltage magnitude or reactive power injection in addition to active power injection regulation at each ac station. However, one of them is usually designated master and the other slave station for load flow study analysis, under master-slave control strategy [21]. Structure of VSC-HVDC system is presented in Fig. 1, while Fig. 2 represents VSC-HVDC transmission system, whose dc link voltage is regulated by one converter and active power flow by the other [27].

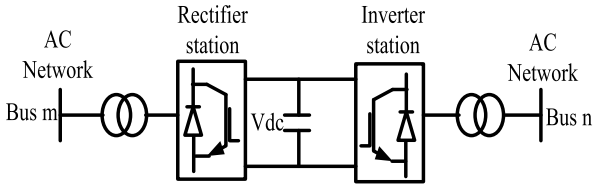

FIGURE 1. Basic structure of VSC-HVDC system.

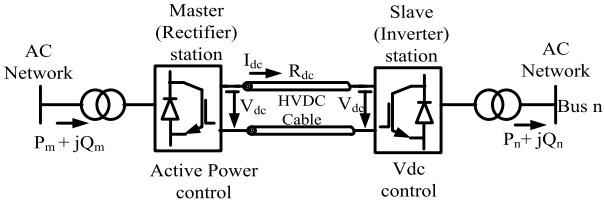

FIGURE 2. Structure of VSC-HVDC transmission system.

A. MODELLING OF VSC-HVDC IN STEADY STATE

In modelling VSC-HVDC in steady state, it is assumed that; the network and converters have balanced three phase voltage whose amplitude and frequency are constant, the current and voltage harmonics for converters are negligible, the dc components have no ripples and, the internal losses of converters are negligible [28]. Therefore, equivalent representation of Fig. 1 can be presented as Fig. 3.

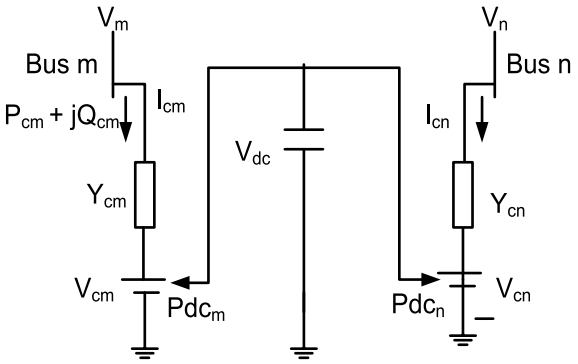

FIGURE 3. Equivalent circuit of VSC-HVDC system.

Phasor voltage of connected converter at bus m and that of bus n from Fig. 3 can be written as (1) and (2), where V_{cm}, V_m, θ_{cm} and θ_m are voltage magnitudes and angles of converter at bus m and that of bus m respectively.

$$V_{cm} = V_{cm}\angle\theta_{cm} = V_{cm}(cos\theta_{cm} + jsin\theta_{cm}) \quad (1)$$

$$V_m = V_m\angle\theta_m = V_m(cos\theta_m + jsin\theta_m) \quad (2)$$

Bus m converter shunt admittance is also given as (3), where G_{cm} and B_{cm} represent conductance and susceptance respectively. The injected complex power into converter at bus m depends on its voltage and shunt current and can be written as (4).

$$Y_{cm} = Y_{cm}\,(cos\theta_{cm} + jsin\theta_{cm}) = G_{cm} + jB_{cm} \quad (3)$$

$$S_{cm} = P_{cm} + jQ_{cm} = V_{cm}I^*_{cm} \quad (4)$$

Therefore, active and reactive power flow into VSC-HVDC can be written as (5) and (6), while injected power at bus m can be written as (7) and (8) [29].

$$P_{cm} = V^2_{cm}G_{cm} + V_{cm}U_m(G_{cm}cos\,(\theta_{cm} - \theta_m) + B_{cm}\sin(\theta_{cm} - \theta_m)) \quad (5)$$

$$Q_{cm} = -V^2_{cm}B_{cm} + V_{cm}U_m(G_{cm}sin\,(\theta_{cm} - \theta_m) - B_{cm}\cos(\theta_{cm} - \theta_m)) \quad (6)$$

$$P_m = V^2_mG_{cm} + V_mV_{cm}(G_{cm}cos\,(\theta_m - \theta_{cm}) + B_{cm}\sin(\theta_m - \theta_{cm})) \quad (7)$$

$$Q_m = -V^2_mB_{cm} + V_mV_{cm}(G_{cm}sin\,(\theta_m - \theta_{cm}) - B_{cm}\cos(\theta_m - \theta_{cm})) \quad (8)$$

Similar equations at bus n can be obtained by interchanging subscripts m with n for (5) to (8). In a situation where the rectifier station performs power control function and inverter station regulates the voltage, the equality constraint equations can be written as (9) – (12), where, P^{spec}_{cm} and Q^{spec}_{cm} are bus m shunt converter specified control active and reactive power.

$$P_{dcm} + P_{dcn} + P_{dcLoss} = 0 \quad (9)$$

$$P_{cm} - P^{spec}_{cm} = 0 \quad (10)$$

$$Q_{cm} - Q^{spec}_{cm} = 0 \quad (11)$$

$$V_n - V^{spec}_n = 0 \quad (12)$$

Likewise, inequality equations can be written as (13) – (15).

$$V^{min}_{cm} \le V_{cm} \le V^{max}_{cm}, \quad V^{min}_{cn} \le V_{cn} \le V^{max}_{cn} \quad (13)$$

$$0 \le \theta_{cm} \le 2\pi, \quad 0 \le \theta_{cn} \le 2\pi \quad (14)$$

$$I_{cm} \le I^{max}_{cm}, \quad I_{cn} \le I^{max}_{cn} \quad (15)$$

Bus m power flow equations are given by (16) and (17) [30].

$$P_m = \sum_{n=1}^{k} |V_m|\,|V_n|\,|Y_{mn}|\cos\,(\theta_{mn} - \theta_m + \theta_n) \quad (16)$$

$$Q_m = \sum_{n=1}^{k} |V_m|\,|V_n|\,|Y_{mn}|\sin\,(\theta_{mn} - \theta_m + \theta_n) \quad (17)$$

Arising from (16) and (17), the resulting modified N-R Jacobean equations to accommodate VSC-HVDC is given by [31], (18), as shown at the bottom of the next page.

As earlier stated, the regulation of active power is achieved at bus m, and that of voltage at n, then $\Delta P_{cm} = P^{spec}_{cm} - P^{cal}_{cm}$, ΔP_n and ΔP_{cn} are not useful in (18). In the same way, ΔQ_n and ΔQ_{cn} are not used because voltage magnitude regulation is done at bus n. From (18), ΔP^{VSC} is active power mismatch, which is obtainable from (19).

$$\Delta P^{VSC} = \Delta P_{cm} - \Delta P_{cn} = P^{spec}_{cm} - P^{cal}_{cm} \quad (19)$$

B. MODELLING OF VSC-HVDC TRANSMISSION LINE

Statically modelling of VSC-HVDC transmission line is crucial to estimation of loss on such line for inclusion in total system loss for optimal placement. The structure of VSC- HVDC system in Fig. 2 is represented by π equivalent of lumped parameters of transmission line in Fig. 4. The sum of admittances between buses m and n and ground is denoted by Y_{mm}, while the admittance between m and n as seeing from

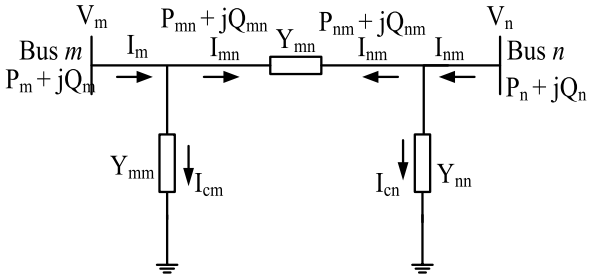

FIGURE 4. π-equivalent of VSC-HVDC transmission system.

m is given by Y_{mn}. The power flow in between bus m and n can be obtained through current and admittance relationship as follows;

$$I_{mn} = I_m - I_{cm} \tag{20}$$
$$I_{mn} = -I_{nm} = Y_{mn}\left(V_m - V_n\right) \tag{21}$$
$$P_{mn} = V_m I_m = \left(Y_{mm} + Y_{mn}\right) V_m^2 - Y_{mn} V_m V_n \tag{22}$$

Both capacitive and inductive components are negligible during steady state for HVDC transmission line interconnecting bus m and n, therefore, (22) can be written as;

$$P_{mn} = \left(G_{mm} + G_{mn}\right) V_m^2 - G_{mn} V_m V_n \tag{23}$$
$$P_{nm} = \left(G_{mm} + G_{mn}\right) V_n^2 - G_{mn} V_m V_n \tag{24}$$

The loss on VDC-HVDC line can be written as;

$$P_{dcL} = P_{mn} + P_{nm} \tag{25}$$
$$P_{dcL} = \left(G_{mm} + G_{mn}\right) V_m^2 + \left(G_{mm} + G_{mn}\right) V_n^2 - 2G_{mn} V_m V_n \tag{26}$$

C. REAL POWER PERFORMANCE INDEX (RPPI)

The change in network parameters consequent contingency occurrence is better evaluated using performance index (PI) because it reveals the deviations in system variables from their initial states. In order to evaluate the influence of VSC-HVDC transmission system on system parameters especially during contingency, real power PI is adopted for ranking of the most severe line outage in this study. Equations describing RPPI are given bellow [32];

$$RPPI = \sum_{m}^{k} \frac{w_p}{2N} \left\{ \frac{P_{mn}}{P_{mn}^l} \right\}^{2N} \tag{27}$$
$$P_{mn}^k = \frac{V_m V_n}{X_{mn}} \tag{28}$$

In the equations, k is bus number, w_p stands for real power weighting factor of non-negative value, penalty function is N, real power on line m-n is P_{mn}, capacity limit of power flow on line m-n is denoted as P_{mn}^l, while V_m, V_n, and X_{mn} are voltages and reactance at/between bus m and n.

III. VSC-HVDC SENSITIVITY BASED OPTIMAL PLACEMENT APPROACH

The presence of shunt devices like VSC usually influences network power loss hence, this parameter is considered as a sensitive factor for optimal placement of VSC-HVDC transmission system in the ac network. This section therefore proposes a sensitive based approach for placement of VSC-HVDC transmission system. The system loss formula is given by (29) [33].

$$P_{Loss} = \sum_{m=1}^{k} \sum_{n=1}^{k} \left[\alpha_{mn}\left(P_m P_n + Q_m Q_n\right) + \beta_{mn}\left(Q_m P_n - P_m Q_n\right)\right] \tag{29}$$
$$\alpha_{mn} = \frac{R_{mn}}{V_m V_n} \cos\left(\theta_m - \theta_n\right) \tag{30}$$
$$\beta_{mn} = \frac{R_{mn}}{V_m V_n} \sin\left(\theta_m - \theta_n\right) \tag{31}$$

P_m, P_n, $Q_m and Q_n$ are the real and imaginary power injected at buses m and n. $\alpha_{mn} and \beta_{mn}$ are loss coefficients while R_{mn} is the real part of bus impedance matrix m *by* n elements obtainable from inverse admittance. Meanwhile, the total loss of a network containing VSC-HVDC transmission system can be taken as the sum of loss on ac network and that of VSC-HVDC transmission line, obtained from (26) and (29) which can be written as (32).

$$P_{TL} = P_{Loss} + P_{dcL} = P_{Loss} + \left(P_{mn} + P_{nm}\right) \tag{32}$$

By taking partial derivatives of (32) with respect to VSC voltage magnitude and angle of control variables respectively, the sensitivity with respect to voltage magnitude denoted

$$\begin{bmatrix} \Delta P_m \\ \Delta P_{cm} \\ \Delta Q_m \\ \Delta Q_{cm} \\ \Delta P^{VSC} \end{bmatrix} = \begin{bmatrix} \frac{\partial P_m}{\partial \theta_m} & \frac{\partial P_m}{\partial \theta_{cm}} & \frac{\partial P_m}{\partial V_m} V_m & \frac{\partial P_m}{\partial V_{cm}} V_{cm} & 0 \\ \frac{\partial P_{cm}}{\partial \theta_m} & \frac{\partial P_{cm}}{\partial \theta_{cm}} & \frac{\partial P_{cm}}{\partial V_m} V_m & \frac{\partial P_{cm}}{\partial V_{cm}} V_{cm} & 0 \\ \frac{\partial Q_m}{\partial \theta_m} & \frac{\partial Q_m}{\partial \theta_{cm}} & \frac{\partial Q_m}{\partial V_m} V_m & \frac{\partial Q_i}{\partial U_{ci}} V_{cm} & 0 \\ \frac{\partial Q_{cm}}{\partial \theta_m} & \frac{\partial Q_{cm}}{\partial \theta_{cm}} & \frac{\partial Q_{cm}}{\partial V_m} V_m & \frac{\partial Q_{cm}}{\partial V_{cm}} V_{cm} & 0 \\ \frac{\partial P^{VSC}}{\partial \theta_m} & \frac{\partial P^{VSC}}{\partial \theta_{cm}} & \frac{\partial P^{VSC}}{\partial V_m} V_m & \frac{\partial P^{VSC}}{\partial V_{cm}} V_{cm} & \frac{\partial P^{VSC}}{\partial V_{cn}} \end{bmatrix} \begin{bmatrix} \Delta\theta_m \\ \Delta\theta_{cm} \\ \frac{\Delta V_m}{V_m} \\ \frac{\Delta V_{cm}}{V_{cm}} \\ \Delta\theta_{cn} \end{bmatrix} \tag{18}$$

by x and that of angle of control denoted by y can be obtained as follows. That is, sensitivity with respect to voltage magnitude V_{cm}, at $V_{cm} = 0$ is denoted by x and that of control angle θ_{cm}, at $\theta_{cm} = 0$ is denoted by y.

$$x = \frac{\partial P_{TLoss}}{\partial V_{cm}}|_{V_{cm}=0} \tag{33}$$

$$y = \frac{\partial P_{TLoss}}{\partial \theta_{cm}}|_{\theta_{cm}=0} \tag{34}$$

x and y can be obtained from (35) and (36) resulting from power loss and converter power equations.

$$\begin{aligned} x &= \frac{\partial P_{TLoss}}{\partial V_{cm}}|_{V_{cm}=0} = \frac{\partial P_{Loss}\partial P_{cm}}{\partial P_{cm}\partial V_{cm}}|_{V_{cm}=0} + \frac{\partial P_{Loss}\partial P_{cn}}{\partial P_{cn}\partial V_{cn}}\Big|_{V_{cn}=0} \\ &+ \frac{\partial P_{Loss}\partial Q_{cm}}{\partial Q_{cm}\partial V_{cm}}\Big|_{V_{cm}=0} + \frac{\partial P_{Loss}\partial Q_{cn}}{\partial Q_{cn}\partial V_{cn}}\Big|_{V_{cn}=0} \\ &+ \left(\frac{\partial P_{mn}}{\partial V_m} + \frac{\partial P_{mn}}{\partial V_n}\right)\Big|_{V_{cm},\, V_{cn}=0} \end{aligned} \tag{35}$$

$$\begin{aligned} y &= \frac{\partial P_{TLoss}}{\partial \theta_{cm}}|_{\theta_{cm}=0} = \frac{\partial P_{Loss}\partial P_{cm}}{\partial P_{cm} V_{cm}\partial \theta_{cm}}|_{\theta_{cm}=0} \\ &+ \frac{\partial P_{Loss}\partial P_{cn}}{\partial P_{cn} V_{cn}\partial V_{cn}}\Big|_{\theta_{cn}=0} + \frac{\partial P_{Loss}\partial Q_{cm}}{\partial Q_{cm} V_{cm}\partial \theta_{cm}}\Big|_{\theta_{cm}=0} \\ &+ \frac{\partial P_{Loss}\partial Q_{cn}}{\partial Q_{cn} V_{cn}\partial \theta_{cn}}\Big|_{\theta_{cn}=0} + \left(\frac{\partial P_{mn}}{V_m\partial \theta_m} + \frac{\partial P_{nm}}{V_n\partial \theta_n}\right)\Big|_{\theta_m,\theta_{n=0}} \end{aligned} \tag{36}$$

The resultant $\frac{\partial P_{cm}}{\partial V_{cm}}\Big|_{V_{cm}=0}$, $\frac{\partial P_{cn}}{\partial V_{cn}}\Big|_{V_{cn}=0}$, $\frac{\partial P_{cm}}{V_{cm}\partial \theta_{cm}}\Big|_{\theta_{cm}=0}$, and $\frac{\partial P_{cn}}{V_{cn}\partial \theta_{cn}}\Big|_{\theta_{cn}=0}$ are obtainable from (5) and also by considering bus n, with recourse to VSC-HVDC control factors, presented as;

$$\frac{\partial P_{cm}}{\partial V_{cm}}\Big|_{V_{cm}=0} = V_m\,(G_{cm}cos\theta_m - B_{cm}sin\theta_m) \tag{37}$$

$$\frac{\partial P_{cn}}{\partial V_{cn}}\Big|_{V_{cn}=0} = V_n(G_{cn}cos\theta_n - B_{cn}sin\theta_n) \tag{38}$$

$$\frac{\partial P_{cm}}{V_{cm}\partial \theta_{cm}}\Big|_{\theta_{cm}=0} = V_m(G_{cm}sin\theta_m + B_{cm}cos\theta_m) \tag{39}$$

$$\frac{\partial P_{cn}}{V_{cn}\partial \theta_{cn}}\Big|_{\theta_{cn}=0} = V_n(G_{cn}sin\theta_n + B_{cn}cos\theta_n) \tag{40}$$

In the same way, corresponding derivatives of reactive power for $\frac{\partial Q_{cm}}{\partial V_{cm}}\Big|_{V_{cm}=0}$, $\frac{\partial Q_{cn}}{\partial V_{cn}}\Big|_{V_{cn}=0}$, $\frac{\partial Q_{cm}}{V_{cm}\partial \theta_{cm}}\Big|_{\theta_{cm}=0}$, and $\frac{\partial Q_{cn}}{V_{cn}\partial \theta_{cn}}\Big|_{\theta_{cn}=0}$ are obtainable from (6) and by considering bus n, with respect to VSC-HVDC control variables as follows;

$$\frac{\partial Q_{cm}}{\partial V_{cm}}\Big|_{V_{cm}=0} = V_m\,(G_{cm}sin\theta_m + B_{cm}cos\theta_m) \tag{41}$$

$$\frac{\partial Q_{cn}}{\partial V_{cn}}\Big|_{V_{cn}=0} = V_n(G_{cn}sin\ theta_n + B_{cn}cos\theta_n) \tag{42}$$

$$\frac{\partial Q_{cm}}{V_{cm}\partial \theta_{cm}}\Big|_{\theta_{cm}=0} = V_m(G_{cm}cos\theta_m - B_{cm}sin\theta_m) \tag{43}$$

$$\frac{\partial Q_{cn}}{V_{cn}\partial \theta_{cn}}\Big|_{\theta_{cn}=0} = V_n(G_{cn}cos\theta_n - B_{cn}sin\theta_n) \tag{44}$$

The derivatives $\frac{\partial P_{mn}}{\partial V_m}\Big|_{V_m=0}$ *and* $\frac{\partial P_{nm}}{\partial V_n}\Big|_{V_n=0}$ representing loss components of voltage magnitude are obtained from (23) and (24), respectively but derivatives for the loss angle components equals zero as a result of dc components, hence;

$$\frac{\partial P_{mn}}{\partial V_m}\Big|_{V_m=0} = -V_n G_{mn} \tag{45}$$

$$\frac{\partial P_{nm}}{\partial V_n}\Big|_{V_n=0} = -V_m G_{mn} \tag{46}$$

Also, the following are obtained from (29),

$$\frac{\partial P_{Loss}}{\partial P_m} = 2\sum_{m=1}^{k} \alpha_{mn}P_n - \beta_{mn}Q_n \tag{47}$$

$$\frac{\partial P_{Loss}}{\partial P_n} = 2\sum_{n=1}^{k} \alpha_{mn}P_m + \beta_{mn}Q_m \tag{48}$$

$$\frac{\partial P_{Loss}}{\partial Q_m} = 2\sum_{m=1}^{k} \alpha_{mn}Q_n + \beta_{mn}P_n \tag{49}$$

$$\frac{\partial P_{Loss}}{\partial Q_n} = 2\sum_{n=1}^{k} \alpha_{mn}Q_m - \beta_{mn}P_m \tag{50}$$

Therefore, sensitivity factors x and y are obtained from (33) and (34) by substituting (37) to (50) in (35) and (36).

A. UNIQUE CONSIDERATIONS FOR APPLICATION OF SENSITIVITY BASED OPTIMAL PLACEMENT METHOD

In order to apply this sensitivity based approach for optimal placement of VSC-HVDC transmission system, the following are applied [33], [34].

- Line with minimum loss sensitivity value with respect to control voltage magnitude is considered for VSC-HVDC transmission system placement.
- Line with highest absolute sensitivity value regarding voltage angle control value is used in placement.
- Any lines containing tap changing transformer components will not be the choice placement of VSC-HVDC system no matter the sensitivity, subsequent in sensitivity ranking will be the choice.
- Similarly, lines adjacent to buses installed with compensating shunt elements are also not good locations for placement, consideration must be accorded the next line on the ranking.

IV. RESULTS AND DISCUSSIONS

VSC-HVDC transmission system incorporated into an ac network based on sensitivity optimization technique is presented as a solution to contingency management in this study. System performance under outage of the most severe ranked contingency line based on RPPI is evaluated. The placement approach and effectiveness of VSC-HVDC transmission system for contingency alleviation are demonstrated on IEEE 6 and 30 bus network systems.

A. OPTIMAL PLACEMENT OF VSC-HVDC TRANSMISSION SYSTEMS

Total loss of the system containing VSC-HVDC transmission system was differentiated with respect to voltage magnitude and angle of control variables and the sensitivities obtained are denoted x and y respectively. However, for effective placement, the sensitivity regarding voltage magnitude must be predominantly negative, while the resulting absolute value of sensitivity for voltage angle control should be the largest. This implies that highest negative value of sensitivity factor x determines the optimal location of VSC-HVDC transmission system. Regarding voltage angle derivative however, the transmission line where highest absolute value of sensitivity factor y occurs determines the optimal location.

1) VSC-HVDC LOCATION FOR IEEE 6 BUS NETWORK

Fig. 5 presents the sensitivity factors represented by x_6 and y_6 for IEEE 6 bus system, as obtained in this study. Highest negative value of x occurred on transmission line 5-6, while maximum absolute value of y also occurred on same line, having taken the unique considerations into cognizance. These values are -4.4416 and 4.4385 for x_6 and y_6 respectively.

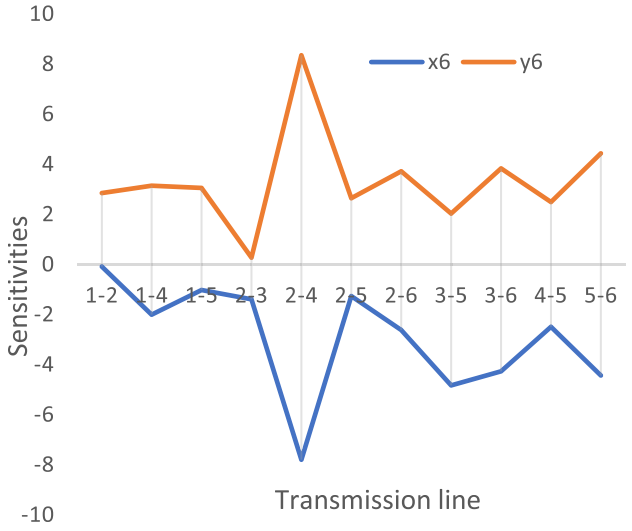

FIGURE 5. Sensitivity factors x_6 and y_6 for optimal placement.

2) VSC-HVDC LOCATION FOR IEEE 30 BUS NETWORK

The sensitivity factor for IEEE 30 bus network is presented in Fig.6. Here x and y are denoted by x_{30} and y_{30} respectively. The highest negative value of x occurred on transmission line 21-22 meaning this is the optimal location for placement of VSC-HVDC transmission system. The maximum absolute value for sensitivity factor y also occurred on same line 21-22. Various values for x and y are well depicted in the figure, but to be precise, the optimal value of x and y which occurred on transmission line 21-22 are -33.6100 and 33.5940 respectively.

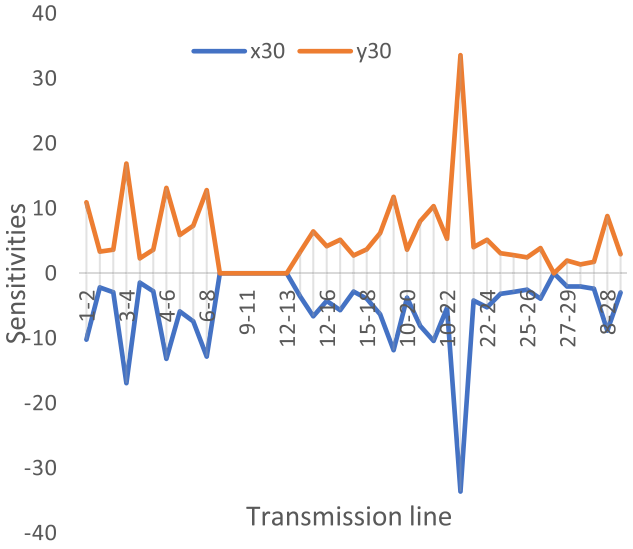

FIGURE 6. Sensitivity factors x_{30} and y_{30} for optimal placement.

B. TEST NETWORK SYSTEMS

IEEE 6 bus network used for analysis in this study is well described in [35], while that of 30 bus network is contained in [32]. The modified configuration is as shown in Fig. 7 and 8 respectively. However, network information, operating settings and line thermal limits are detailed in Appendix 2 of IEEE bus networks data sheet. In brief, bus voltage lower limits for all the buses including slack are taken as 0.95 p.u. and that of upper limit to be 1.05 p.u., with the exception of generator buses whose upper voltage limit is 1.1 p.u. VSC-HVDC transmission system has been used to outrightly replace the existing ac lines 5-6 and 21-22 in the networks as depicted in the figures. These locations are as optimized by the proposed sensitivity method.

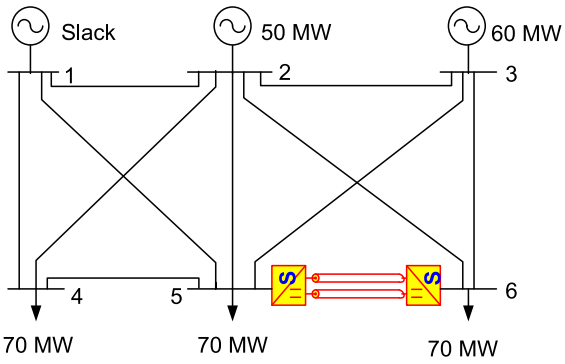

FIGURE 7. Modified IEEE 6 bus test network.

C. SEVERE CONTINGENCY RANKING AND SELECTION

In order to implement contingency ranking and eventual selection, load flow was performed after outage of each transmission line on the test networks prior to placement of VSC-HVDC transmission system. Ranking was done based on sensitivity of outage of each line to the disturbance. Order of ranking was determined by performance index sensitivity

to the various line outages, in descending order from utmost severe to the least. This presents lines 3-6 and 2-5 for bus 6 and 30 respectively, as the most ranked severe contingency as appears on Table 1 [32],[35], which contains the first five ranked severe outage lines.

TABLE 1. Ranking of contingency.

	IEEE 6 Bus			IEEE 30 Bus		
Ranking Order	Line No	Line	RPPI	Line No	Line	RPPI
1	9	3-6	2.3006	5	2-5	321.0613
2	5	2-4	2.1135	9	6-7	262.0340
3	2	1-4	1.2306	14	9-10	258.2439
4	8	3-5	1.1743	2	1-3	247.1413
5	3	1-5	1.1344	4	3-4	243.9255

D. IMPACTS OF VSC-HVDC TRANSMISSION SYSTEM ON NETWORK

The need to optimize network utilization amidst technical and economical restrictions confronted with physical network expansion calls for intensive research into applications of FACTS and HVDC transmission systems. Effects of VSC-HVDC transmission system on ac network especially during line outage contingency has been investigated in the subsequent paragraphs. The investigations were conducted within the attributes of a deregulated and restructured power network.

1) POWER TRANSACTIONS ON 6 BUS NETWORK

Power transactions involving bilateral, simultaneous and multilateral trading were implemented and investigated amidst contingency in this study. By interpretation, power transaction involves trading and wheeling of power among market participants, while contingency in this context implies the outage of a transmission line in the network. Bilateral transaction of 40 MW power between generator bus 2 and load bus 4 is tagged T1, simultaneous transaction of 40 MW power trading between generator bus 2 and load buses 4 and 6 is termed T2, while multilateral transactions of 40 MW power among generator buses 2 & 3 and load buses 4 & 6 are tagged T3 as implemented on the 6 bus system.

2) POWER TRANSACTIONS ON 30 BUS NETWORK

Likewise for the 30 bus system, Bilateral transaction of 40 MW power between generator bus 2 and load bus 20 is named T4, simultaneous transaction of 40 MW power trading between generator bus 5 and load buses 16 and 18 is termed T5, while multilateral transactions of 40 MW power among generator buses 5 & 8 and load buses 15 & 24 are tagged T6 for the purpose of distinction in this study.

E. IEEE 6 BUS TEST SYSTEM VOLTAGE PROFILE WITH AND WITHOUT CONTINGENCY

The impacts of VSC-HVDC transmission line on network bus voltage values during implemented bilateral, simultaneous and multilateral transactions are investigated and presented here.

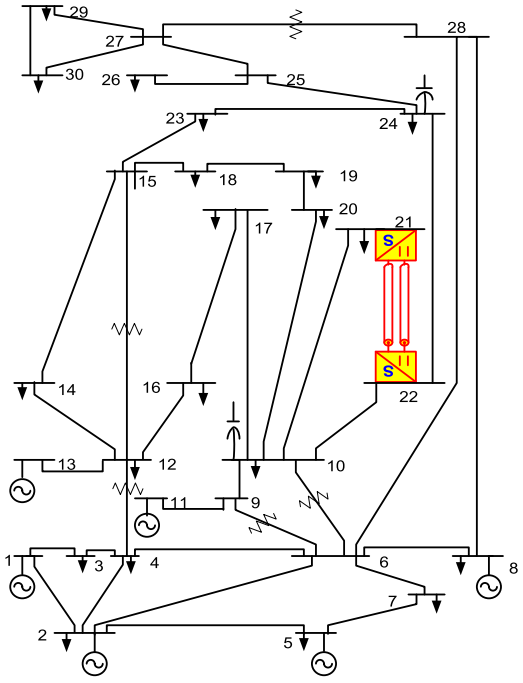

FIGURE 8. Modified IEEE 30 bus test network.

1) BUS VOLTAGE PROFILE WITHOUT TRANSACTION

Contingency involving outage of transmission line 3-6 was created, and its effects observed on the test network bus voltage profile. In Fig. 9, the bus voltage profile for normal network operation, network with line outage contingency as well as compensated power system is clearly depicted. The compensation of network with optimized HVDC system restored voltage deviation that was experienced as a result of basic power flow as well as during severe line outage contingency. As can be seen from Fig. 9, the voltage dipped into lower limit at buses 4, 5 and 6 was restored.

2) BUS VOLTAGE PROFILE DURING TRANSACTION T1

During transaction T1, voltage deviation towards lower limits at buses 4, 5 and 6 was more intense as presented in Fig. 10. The deviation which stood at about 0.98 p.u as a result of 40 MW transaction was further aggravated below this value with occurrence of contingency. However, the deviations were restored on the two occasions, with and without contingency, when HVDC system was incorporated.

3) BUS VOLTAGE PROFILE DURING TRANSACTION T2

During transaction T2, voltage at buses 4, 5 and 6 which hitherto was 0.9828, 0.9829 and 0.9975 p.u. was improved to 0.9841, 1.0000 and 1.0257 p.u. respectively, with HVDC compensation. With occurrence of contingency, these values further deviated to 0.9821, 0.9771 and 0.9990 p.u. at buses 4, 5 and 6 respectively. In Fig. 11, the mitigation impact of an

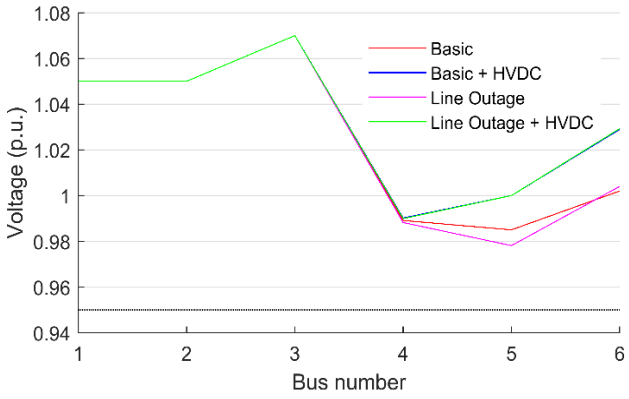

FIGURE 9. Basic Bus voltage profile with and without contingency.

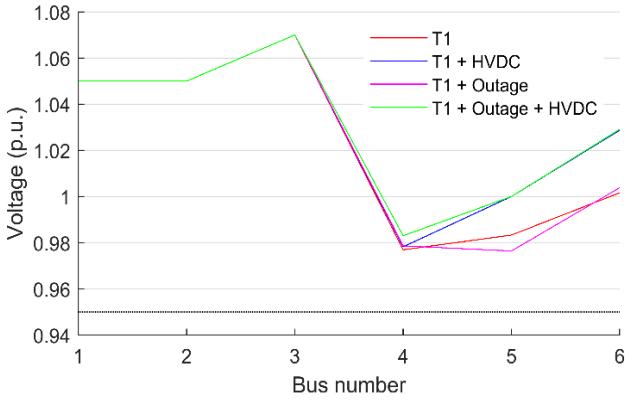

FIGURE 10. Voltage profile with and without contingency during T1.

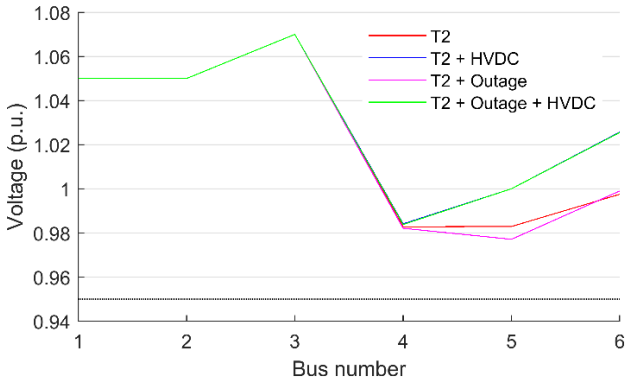

FIGURE 11. Voltage profile with and without contingency during T2.

optimized HVDC system can be succinctly visualized with restoration of these values to 0.9838, 1.0000 and 1.0255 p.u. respectively.

4) BUS VOLTAGE PROFILE DURING TRANSACTION T3

Just like other transactions, voltage profile during multilateral transaction led to deviation of bus voltage at buses 4, 5 and 6 towards lower limits. Similarly, the contingency occurrence here also led to further voltage sags, but these were ameliorated with incorporation of an optimized HVDC system. Fig. 12 presents voltage profile of IEEE 6 bus network during this transaction. During contingency, 0.9776, 0.9763 and 0.9963 p.u. were restored to 0.9781, 1.0000 and 1.0215 p.u. at buses 4, 5, and 6 respectively.

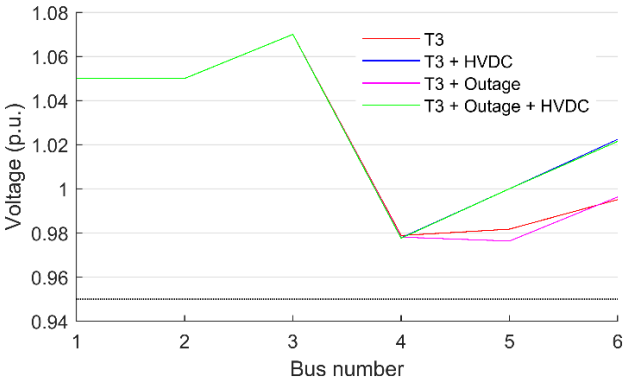

FIGURE 12. Voltage profile with and without contingency during T3.

F. IEEE 6 BUS NETWORK POWER FLOW WITH AND WITHOUT CONTINGENCY

The presence of VSC-HVDC system in an ac network also impacted power flow during various transactions for IEEE 6 bus test system. These are described and reported in the subsequent sections.

1) POWER FLOW WITHOUT TRANSACTIONs

The basic power flow without transaction is depicted in Fig. 13. In Fig 13 (a), the compensation of network with

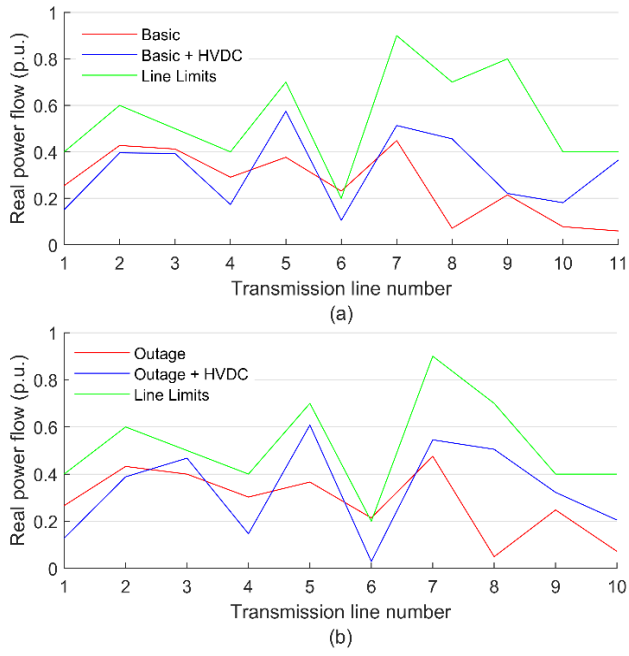

FIGURE 13. Bus 6 network power flow without transaction (a) without contingency, (b) with contingency.

HVDC system resulted into power flow enhancement of the system and restoration of thermal limit violation that occurred on transmission line 2-5. Similar scenario played out in Fig. 13 (b), where the line thermal limit violation was fixed, due to incorporation of optimally placed VSC-HVDC system.

2) POWER FLOW DURING TRANSACTIONs T1

Power flow of the test network during bilateral transaction T1 is depicted in Fig. 14 (a) & (b). Power flow has been enhanced and thermal violation restored just as in the case of basic power flow without trading as presented in Fig. 14 (a). When contingency occurred in the case of Fig. 14 (b), the associated thermal violation was also reinstated. This was achieved through diversion of power to the adjoining lines, interconnecting overloaded line.

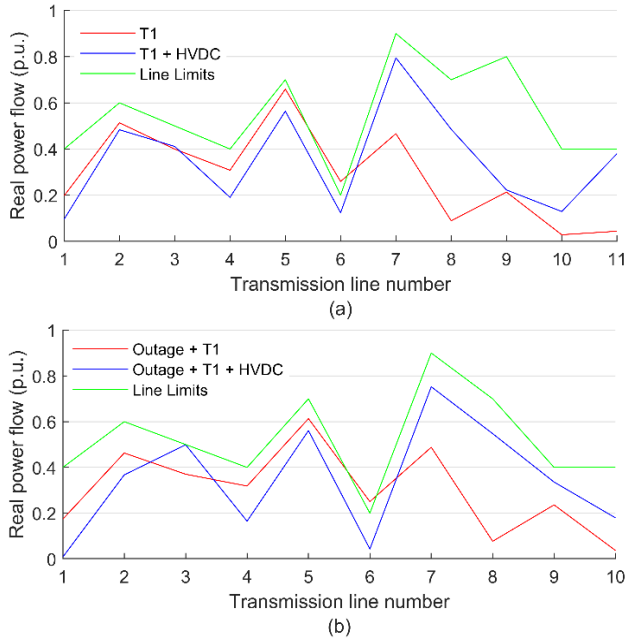

FIGURE 14. Bus 6 network power flow during transaction T1 (a) without contingency, (b) with contingency.

3) POWER FLOW DURING TRANSACTIONs T2

The situation with power flow of the test network during simultaneous transaction T2 as depicted in Fig. 15 (a) & (b) is similar to that of bilateral transaction presented in Fig. 14, but with different power flow magnitude. Both with and without contingency, the thermal violation experienced in the network were ameliorated with compensated system. These are as shown in Fig. 15 (a) and (b).

4) POWER FLOW DURING TRANSACTIONs T3

Multilateral transaction among buses 2, 3, 4 and 6 resulted into thermal violation of both transmission lines 2-3 and 2-5 without and with contingency occurrence. This is presented in Fig. 16 (a) and (b). The capability of HVDC system in mitigating the contingency is also demonstrated

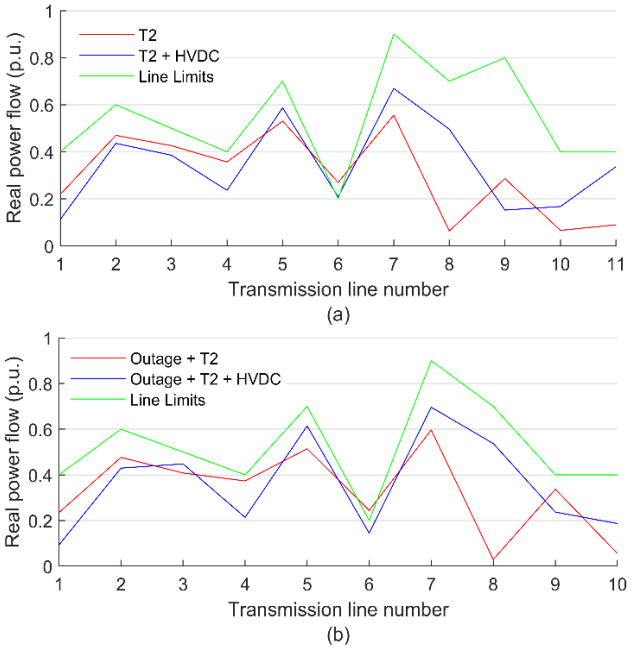

FIGURE 15. Bus 6 network power flow during transaction T2 (a) without contingency, (b) with contingency.

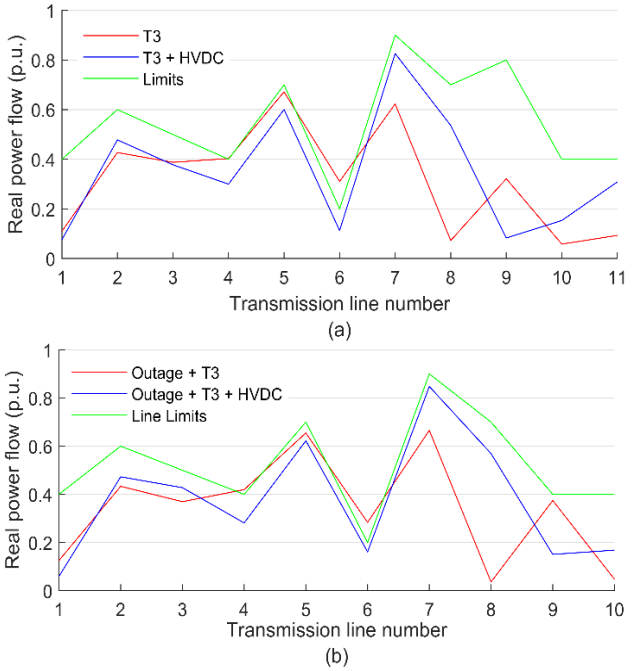

FIGURE 16. Bus 6 network power flow during transaction T3 (a) without contingency, (b) with contingency.

in the figures, where, thermal overloading was isolated with the presence of an optimized HVDC system. Loading on the lines 2-3 and 2-5 which were 0.4029 and 0.3108 p.u. without contingency were restored to 0.2999 and 0.1127 p.u. respectively. These values which were 0.4196 and 0.6657 p.u. with contingency occurrence were also restored to 0.2814 and 0.1611 p.u. respectively.

G. IEEE 30 BUS VOLTAGE PROFILE WITH AND WITHOUT CONTINGENCY

The impacts of VSC-HVDC transmission line on network bus voltage values during implemented bilateral, simultaneous and multilateral transactions n IEEE 30 bus system are investigated and presented in here.

1) BUS VOLTAGE PROFILE WITHOUT TRANSACTIONS

Outage of transmission line 2-5 contingency was created here, and effects observed on the test network bus voltage profile. Fig. 17 presents bus voltage profile for normal power flow and flow during outage of line 2-5. During normal power flow, voltage profile deviation was pronounced in the upper region of the network where generators are not located. The deviation is glaring from bus 15 up to 30. However, replacement of ac transmission line 21-22 with VSC-HVDC transmission line minimizes this deviation as shown in the figure.

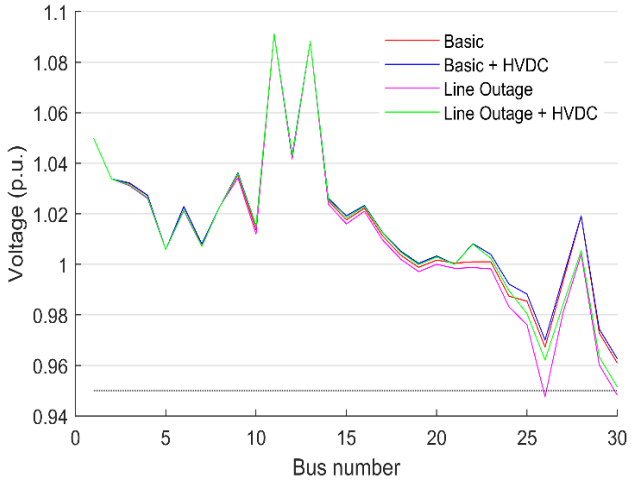

FIGURE 17. Bus voltage profile with and without contingency.

With the occurrence of contingency, bus limit violation occurred at buses 26 and 30 as indicated in magenta color in Fig. 17. Presence of HVDC in the network not only minimized bus voltage deviation but also restored violated bus limits. Bus 26 and 30 had their terminal voltage restored to 0.9621 and 0.9514 p.u. from 0.9476 and 0.9482 p.u. respectively as indicated by green color in the figure.

2) BUS VOLTAGE PROFILE FOR BILATERAL TRANSACTION T4

Generator bus 2 and load bus 20 engaged in bilateral transfer of 40 MW power during T4. Bilateral transaction involves power trading between a seller and a buyer in a deregulated power sector. Bus voltage profile associated with this transaction is depicted in Fig. 18. In this transaction, bus voltage profile deviation is more pronounced compared to voltage profile without transaction for both normal network flow and contingency condition. In each case, voltage profile deviated towards the lower limits. When line 21-22 was replaced

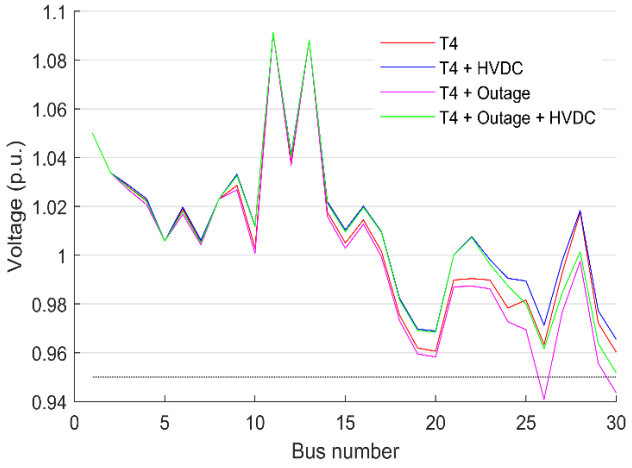

FIGURE 18. Bus voltage profile for bilateral transaction T4.

with HVDC, the deviation was minimized as evident in the figure. Line with blue color indicate this as compared with red color line.

Bus voltage limit was violated at bus 26 and 30 when contingency occurred during this transaction. The depth of voltage dip at these buses transcend the depth when there were no transactions. However, the inclusion of HVDC restored this violation to the limit. Voltage at bus 26 was sagged to 0.9408, and that of bus 30 to 0.9435 p.u. but restored to 0.9616 and 0.9517 p.u. respectively with presence of HVDC system.

3) BUS VOLTAGE PROFILE FOR SIMULTANEOUS TRANSACTION T5

Simultaneous transaction involves dispatching of power from the same generator to two or more load centres concurrently. This was also implemented with generator bus 2 transferring 40 MW of power to load buses 16 and 18 at the same time. The response of network bus to this transaction is shown in Fig. 19. Voltage deviation profile is a bit relax unlike T4 because wheeling of power to these load buses flow through different paths as can be inferred from Fig. 8. In the case of T4, the dispatch was from single seller to another single buyer but for T5 it was from single seller to two different buyers at the same time. This created room for flexibility in power flow.

Just like previous transactions, the inclusion of HVDC in ac network provided support for bus voltage as can be seen in the figure. Bus voltage at bus 21 was held around 1.0 p.u. while that of bus 22 was held constant at 1.0 p.u. This is depicted by blue and green line of the curves. As usual, voltage limit violation resulted from outage of line 2-5, but the violation at buses 26 and 30 was restored in this case as well. Voltages were reduced to 0.9434 p.u. at bus 26 and to 0.9456 p.u. at bus 30, however, with presence of HVDC in the tested ac network the violations were restored to 0.9615 p.u. and 0.9516 p.u. respectively.

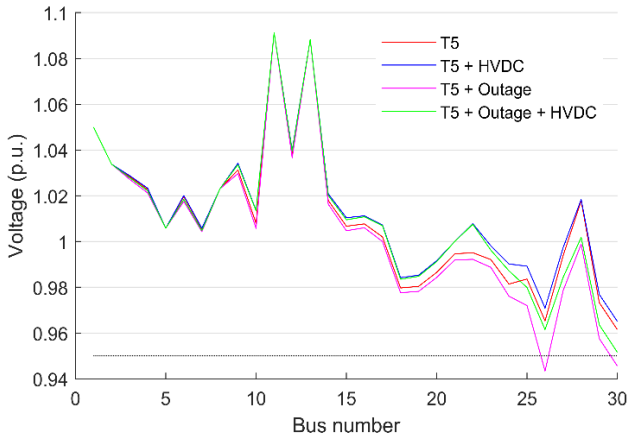

FIGURE 19. Bus voltage profile for simultaneous transaction T5.

4) BUS VOLTAGE PROFILE FOR MULTILATERAL TRANSACTION T6

Multilateral transaction involves multiple sellers and multiple buyer for concurrent power wheeling in a restructured power system. This type of transaction was also implemented, and the voltage profile obtained for 40 MW trading is as shown in Fig. 20. Multilateral transaction is more demanding on terminal voltage because of concurrent wheeling of power to and from multiple buses. The response of bus voltage profile to this transaction is as shown. Between bus one and thirteen where generators are located, the profile deviation was controlled but reactive power control capability of these generators has been weakened in the upper region of the test network thereby giving room for significant deviation in voltage profile in the region, as experienced during T6 without contingency.

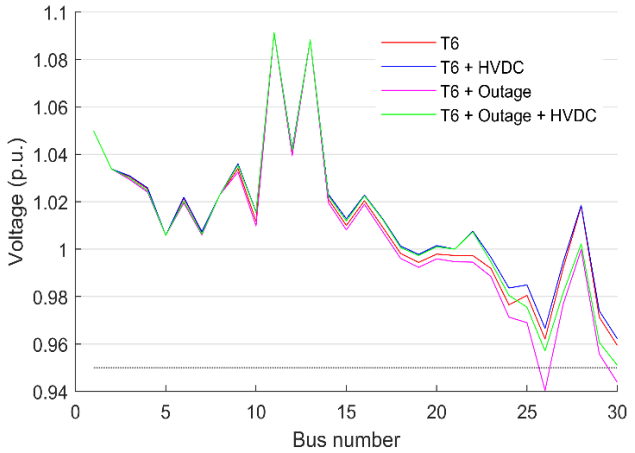

FIGURE 20. Bus voltage profile for multilateral transaction T6.

When contingency occurred, the reactive power control responsible for bus voltage regulation was loss totally thereby leaving bus 26 and 30 vulnerable. These buses operated below their lower limit bound at 0.9404 and 0.9438 p.u. respectively. However, with embedded HVDC system in the test network, these values were improved to 0.9571 and 0.9510 p.u. for buses 26 and 30 respectively.

H. IEEE 30 BUS NETWORK POWER FLOW WITH AND WITHOUT CONTINGENCY

The impacts of VSC-HVDC system on network power flow during various transactions as described are reported in this section. Power flow control capability of VSC-HVDC system is reported in this section.

1) POWER FLOW WITHOUT TRANSACTIONS

Fig. 21 presents transmission line flows without power transaction. In Fig. 21(a), power flow without contingency is presented. HVDC transmission system alters the flow pattern when incorporated to replace transmission line 21-22 outrightly. The improvement in the flows on the transmission lines in the vicinity of lines 21-22 are of great interest. More flows occurred on lines 10-21 and 10-22 but without thermal limit violation. Besides these lines, the influence of flow enhancement capability of HVDC system were also felt by other transmission lines.

When contingency occurred as presented in Fig. 21(b), thermal limit violation occurred on transmission lines 4-6, 5-7 and 25-27 as indicated by line numbers, 6, 8, and 35 respectively. The overloading of these lines resulted from addition flow on them due to outage of line 2-5. With the presence of HVDC transmission system in the network however, power flows were diverted to adjoining interconnected transmission lines, thereby forcing the lines operation within the limits. These initial flows which were 0.6781, 0.8639 and 0.1515 p.u. on lines 6, 8 and 35 reduced to 0.5137, 0.5174 and 0.0355 p.u. respectively. This is well depicted in the figure.

2) POWER FLOW DURING BILATEAL TRANSACTION T4

Power trading due to liberalization constitutes additional burden to network operations which hitherto have been in the region of their limits. When there was no trading as presented in Fig. 21(a), none of transmission line limits were violated however, with 40 MW power transfer from generator 2 to load bus 20, thermal violation of lines 9-10, 18-19 and 10-20 occurred as presented in Fig. 22(a) in addition to increase in power flow on other transmission lines. These line overloads were properly controlled by HVDC transmission system as clearly presented in the figure. These loads were reduced from 0.3020, 0.1719 and 0.3596 p.u. to 0.2507, 0.1207 and 0.2324 p.u. agreeable to line limits 0.2560, 0.1280 and 0.2500 p.u. respectively for these lines.

In Fig, 22(b), the magnitude and number of occurrences of thermal overload increased due to outage of line 2-5. Line numbers 5, 6, 8, 17, 21, 22, 24, and 35 were affected as presented in the figure. Notwithstanding the overloads created by this contingency, HVDC system adequately controlled and restored the violations when it was incorporated into the ac network. In this condition, 0.7829, 0.7810, 0.8648, 0.3135, 0.2142, 0.1772, 0.3542 and 0.1882 p.u. controlled to

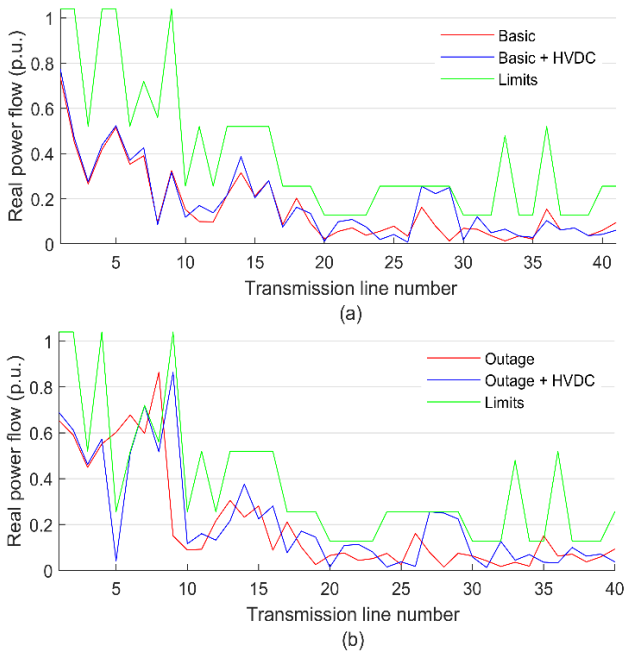

FIGURE 21. Network power flow without transaction (a) without contingency, (b) with contingency.

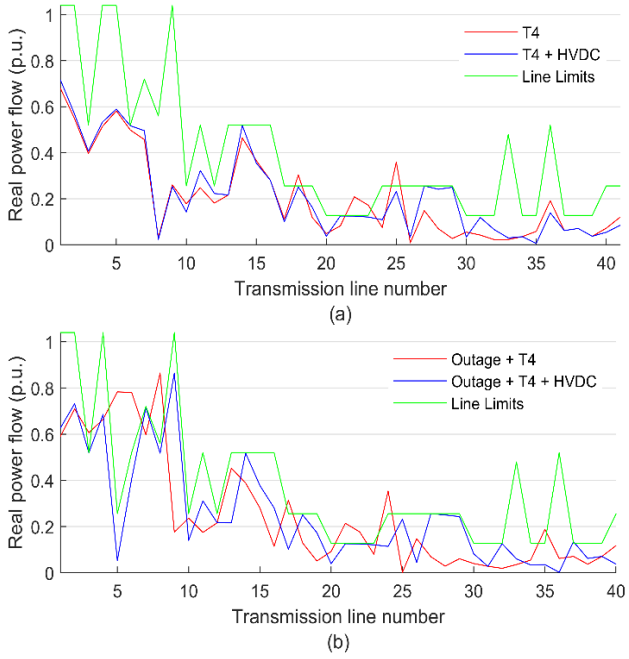

FIGURE 22. Network power flow for bilateral transaction (a) T4 without contingency, (b) T4 with contingency.

0.0527, 0.4055, 0.7143, 0.1023, 0.0391, 0.1258, 0.1212 and 0.0339 p.u. for lines 6-28, 2-6, 5-7, 12-14, 15-18, 19-20, and 25-27 respectively.

3) POWER FLOW DURING SIMULTANEOUS TRANSACTION T5

Impacts of simultaneous transfer of power was as not as severe as that of bilateral trading on the network system. Thermal overloading of lines 18 and 22 resulted from this transaction without contingency as presented in Fig. 23(a). The flows which exceeded the rated values of 0.2560 and 0.1280 p.u. with 0.0109 and 0.0535 p.u. were controlled to 0.2255 and 0.1218 p.u. respectively, when HVDC transmission system was used to replace ac line 21-22 in the network.

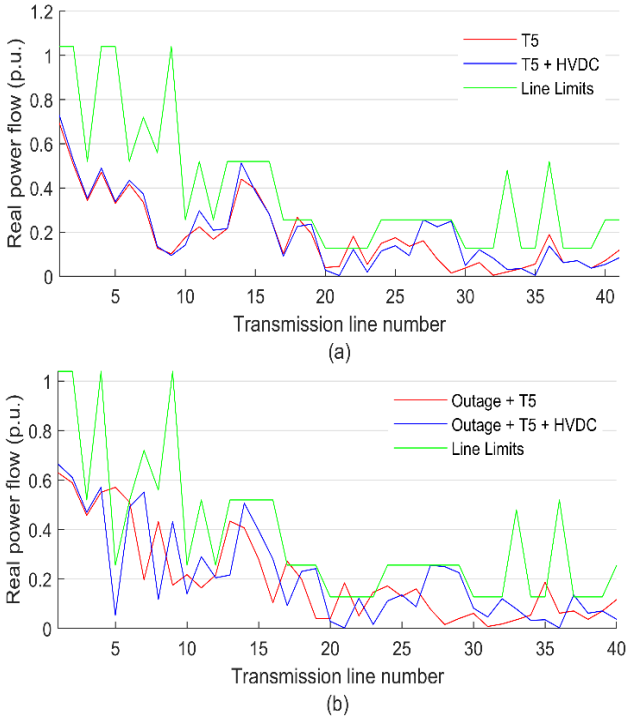

FIGURE 23. Network power flow for simultaneous transaction (a) T5 without contingency, (b) T5 with contingency.

The occurrence of line outage contingency aggravated thermal limit violations. Transmission lines 6-28, 16-17, 18-19 and 25-27 had their thermal limit violated because shed off power that would have otherwise flown through line 2-5 flew through them. From Fig. 23(b), the flows which were 0.5709, 0.1845, 0.1465 and 0.1873 p.u. were properly controlled to 0.0531, 0.0023, 0.0164 and 0.0355 p.u. respectively when HVDC system was installed on the network.

4) POWER FLOW DURING MULTILATERAL TRANSACTION T6

Apart from the previous trading, multilateral power transaction is another type of transaction which occurs in a deregulated network. The network responses to the implementation of 40 MW power transfer from seller generators buses 5 and 8 to buyer load buses 15 and 24 are as depicted in Fig. 24 (a) and (b). Transmission line number 18 which was overloaded during this trading was relieved with presence of HVDC system. No other line thermal violation was recorded meaning that the magnitude and the nature of this trading impacted less on the network as shown in Fig. 24(a).

During contingency however, transmission lines 5-7, 12-14, and 25-27 suffered thermal overload. With thermal ratings of 0.5600, 0.2500, and 0.1280 p.u., power flow on

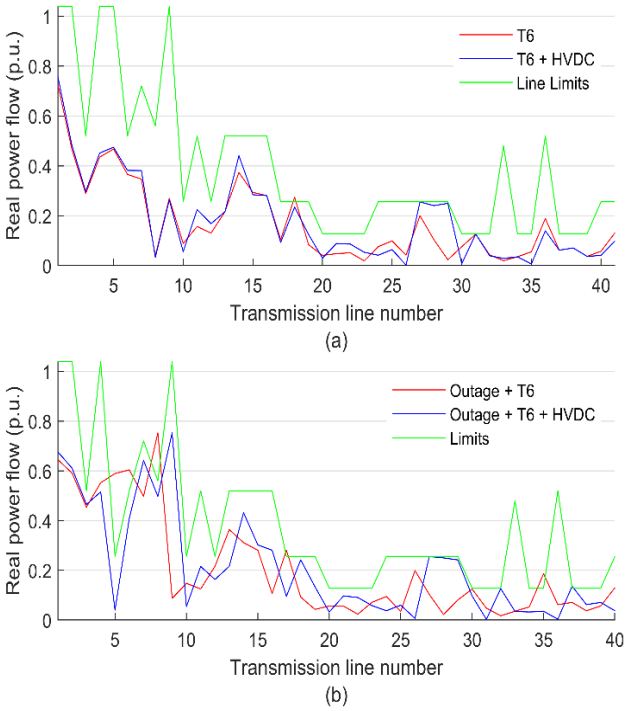

FIGURE 24. Network power flow for multilateral transaction (a) T6 without contingency, (b) T6 with contingency.

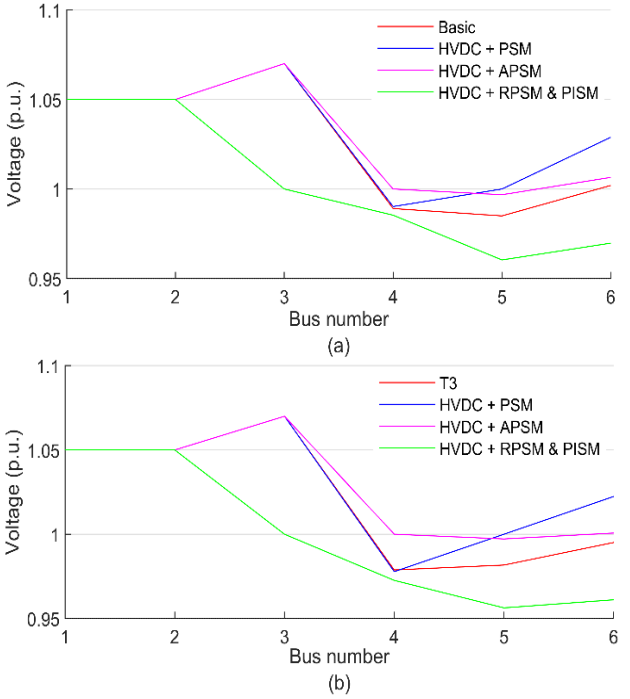

FIGURE 25. Network voltage profile with different placement methods without contingency (a) basic power flow, (b) multilateral transaction T3.

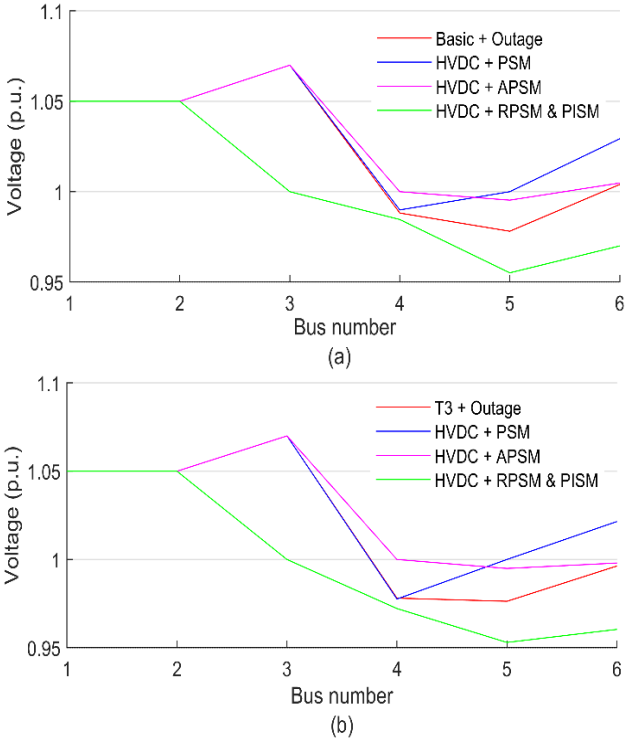

FIGURE 26. Network voltage profile with different placement methods with contingency (a) basic power flow, (b) multilateral transaction T3.

these lines were 0.7533, 0.2815 and 0.1860 p.u. respectively. These flows were controlled to fall within the limits, thereby suppressing these values to 0.4974, 0.0951, and 0.0355 p.u. when line 21-22 was replaced with HVDC transmission system.

I. COMPARISON OF THE PROPOSED METHOD WITH OTHER SENSITIVITY PLACEMENT APPROACHES

This method, which is unique in the sense that it incorporates power loss on line containing VSC-HVDC system, into system total power loss is termed power loss with device line loss sensitivity method (PLWDLLSM or PSM) for simplicity of representation. This is compared with three other sensitivity placement approaches namely; total active power sensitivity but without inclusion of loss on the line containing device (APSM), total reactive power sensitivity (RPSM), and performance index sensitivity (PISM) approaches. This was with a view to showcasing the performance of this method as compared other similar methods. In performance comparison with IEEE 6 bus network, RPSM and PISM identified transmission line 3-6 as the optimized location, while line 4-5 was the optimal location for APSM method.

1) COMPARISON OF IEEE 6 BUS VOLTAGE PROFILE WITH DIFFERENT SENSITIVITY PLACEMENT METHODS

Fig. 25 presents voltage profile of 6 bus test system with different placement approaches. During basic power flow, as shown in Fig. 25 (a), placement of HVDC system with both RPSM and PISM methods resulted into a diminished voltage profile compared uncompensated system. APSM placement method slightly improved voltage profile of a compensated network but not as improved as that of the proposed

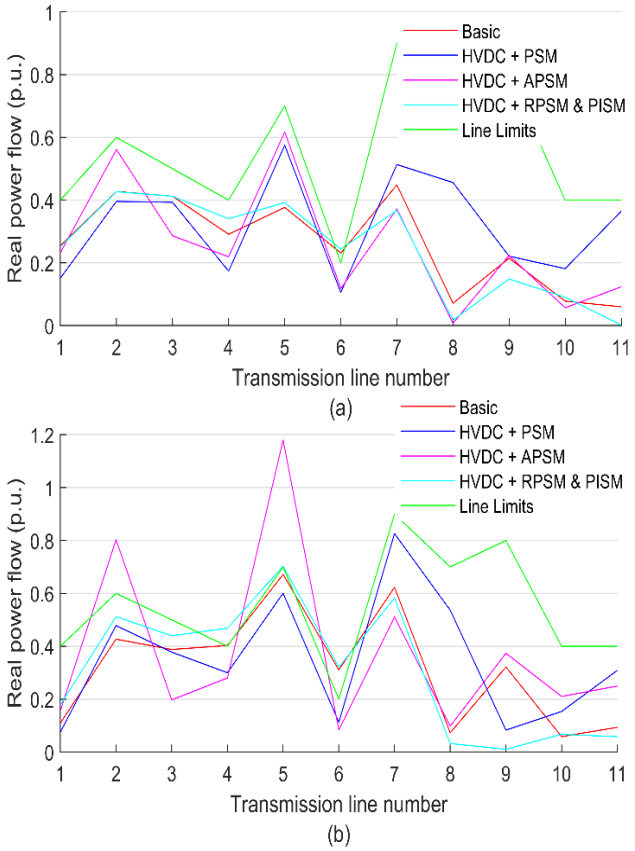

FIGURE 27. Network power flow with different placement methods without contingency (a) basic power flow, (b) multilateral transaction T3.

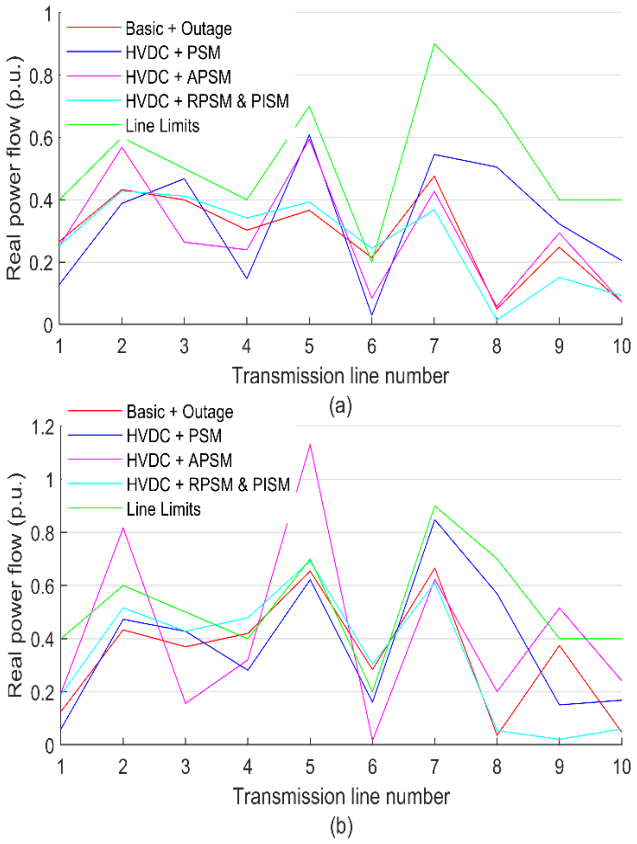

FIGURE 28. Network power flow with different placement methods with contingency (a) basic power flow, (b) multilateral transaction T3.

PSM method. During this situation, the values of bus voltage at 5 and 6 improved to 1.0000 and 1.0289 p.u. with PSM as compared 0.9953 and 1.0048 p.u. using APSM approach. The situation in Fig. 25 (b), during multilateral transaction is similar to that of Fig. 25 (a), where the performance of HVDC system with PSM approach supersede other methods. With the occurrence of contingency as presented in Fig. 26 (a) & (b), PSM placement method sustained its performance through enhancement of bus voltage profile as compared other methods. In both scenarios, PSM outperformed APSM, RPSM and PISM placement approaches in contingency mitigation.

2) COMPARISON OF IEEE 6 BUS ACTIVE POWER FLOW WITH DIFFERENT PLACEMENT METHODS

The network response to different mode of placement of HVDC system in terms of active power flows is compared in Fig. 27 (a) and (b). In Fig. 27 (a), both APSM and PSM method restored thermal violation on transmission line 2-5, however, PSM not only properly ameliorated the violated thermal limits, it also enhanced power flow more than APSM method. Placement achieved via RPSM and PISM method aggravated thermal limit violation on transmission line number 6. During this flow analysis, PSM improved total power flow to 3.5314 p.u. from 2.8673 p.u., while APSM and RPSM/PISM impaired total flow to 2.8177 p.u. and 2.6922 p.u. respectively. When multilateral transaction occurred as presented in Fig. 27 (b), all other placement methods resulted into thermal limit violation except PSM method. APSM resulted into overloading of line 2, 4, and 5, while RPSM and PISM led to thermal violation on line 4 and 6. Total power flow of uncompensated system which was 3.4789 p.u. was controlled to 3.8527, 4.1415 and 3.3723 p.u. by PSM, APSM and RPSM/PISM approach respectively. In Fig. 28 (a) and (b), the response of network to these various placement approaches are presented during contingency occurrence. In Fig. 28 (a), placement of HVDC system with RPSM/PISM could not remove thermal overload of line 2-5 unlike PSM method. In Fig. 28 (b), this placement approach resulted into thermal overload of additional transmission line 2-3.

Similarly, APSM method resulted into thermal violation of line numbers 2 and 5, whereas, the proposed placement approach controlled power flow and kept it within the limit in addition to flow enhancement. Besides, this approach properly controlled network contingency despite multilateral trading. These scenarios are the replica of network behavior even in higher network bus systems because the propose method is scalable.

V. CONCLUSION

Contingency control capability of VSC-HVDC system integrated into an ac network has been investigated in this study. Equivalent π model representation of transmission line lump parameters were deployed with a view to obtaining loss on the line containing VSC-HVDC system. These were mathematically embedded with steady state model equations of VSC-HVDC system for determination of its optimal location for placement in an ac network. The objective of using sensitivity analysis based on controlled parameters of VSC was discerned through consideration for the impacts of shunt devices on network loss characteristics. However, an n-1 transmission line outage contingency was created based on the most severe ranked outage line. Real power performance index ranking of the most severe outage line was adopted because of its effectiveness in identification of the critical line for contingency implementation. Various power transactions which characterised deregulated and restructured power network were implemented on the standard IEEE 6 and 30 bus systems, used in the analyses. The incorporation of VSC-HVDC system in-between ac buses in a network using the proposed approach minimized bus voltage profile deviation for steady state and restored violated bus voltage limits during contingencies. Power flow were enhanced during steady state and thermal limit violation occasioned by contingencies were adequately controlled. During bilateral, simultaneous and multilateral transactions however, the presence of this HVDC in the ac network not only damped the impactful effects of power transfers on network characteristics, but also controlled both voltage and thermal limit violations as a result of associated contingencies. Unlike other sensitivity-based approaches, the impacts of the loss especially of the line containing the device on the optimization process is a unique hallmark here and it has resulted into better performance of this approach compared others. Therefore, VSC-HVDC system incorporated into ac network using this approach outperformed other sensitivity-based methods as presented. Besides, this method has the capacity to greatly influence system performance and it stands a solution to problems of contingency especially in a deregulated and restructured power network.

REFERENCES

[1] Y. Huang, Q. Xu, S. Abedi, T. Zhang, X. Jiang, and G. Lin, "Stochastic security assessment for power systems with high renewable energy penetration considering frequency regulation," *IEEE Access*, vol. 7, pp. 6450–6460, 2019, doi: 10.1109/ACCESS.2018.2880010.

[2] C. Rathore, P. B. Thote, S. Kamble, V. Naik, P. Singh, and M. Jukaria, "Transmission network expansion planning considering transmission switching and pumped-storage," in *Proc. IEEE Int. WIE Conf. Electr. Comput. Eng. (WIECON-ECE)*, Dec. 2017, pp. 161–164.

[3] NERC. (2005). *North America Electric Reliability Council: Standard 51, Transmission System Adequacy and Security*. [Online]. Available: www.nerc.com

[4] M. Majidi-Qadikolai and R. Baldick, "Integration of contingency analysis with systematic transmission capacity expansion planning: ERCOT case study," *IEEE Trans. Power Syst.*, vol. 31, no. 3, pp. 2234–2245, May 2016, doi: 10.1109/TPWRS.2015.2443101.

[5] M. Majidi-Qadikolai and R. Baldick, "Reducing the candidate line list for practical integration of switching into power system operation," in *Proc. 22nd Int. Symp. Math. Program.*, Pittsburgh, PA, USA, 2015, pp. 1–15.

[6] H. Peng, M. Su, S. Li, and C. Li, "Static security risk assessment for islanded hybrid AC/DC microgrid," *IEEE Access*, vol. 7, pp. 37545–37554, 2019, doi: 10.1109/ACCESS.2019.2899347.

[7] T. Joseph, C. E. Ugalde-Loo, J. Liang, and P. F. Coventry, "Asset management strategies for power electronic converters in transmission networks: Application to HVDC and FACTS devices," *IEEE Access*, vol. 6, pp. 21084–21102, 2018, doi: 10.1109/ACCESS.2018.2826360.

[8] Imdadullah, S. M. Amrr, M. S. Jamil Asghar, I. Ashraf, and M. Meraj, "A comprehensive review of power flow controllers in interconnected power system networks," *IEEE Access*, vol. 8, pp. 18036–18063, 2020, doi: 10.1109/ACCESS.2020.2968461.

[9] E. Pierri, O. Binder, N. G. A. Hemdan, and M. Kurrat, "Challenges and opportunities for a European HVDC grid," *Renew. Sustain. Energy Rev.*, vol. 70, pp. 427–456, Apr. 2017, doi: 10.1016/j.rser.2016.11.233.

[10] B. Van Eeckhout, D. Van Hertem, M. Reza, K. Srivastava, and R. Belmans, "Economic comparison of VSC HVDC and HVAC as transmission system for a 300 MW offshore wind farm," *Eur. Trans. Electr. Power*, vol. 20, pp. 661–671, Jul. 2010, doi: 10.1002/etep.359.

[11] Y. S. Borovikov, A. S. Gusev, A. O. Sulaymanov, R. A. Ufa, A. S. Vasilev, M. V. Andreev, N. Y. Ruban, and A. A. Suvorov, "A hybrid simulation model for VSC HVDC," *IEEE Trans. Smart Grid*, vol. 7, no. 5, pp. 2242–2249, Sep. 2016, doi: 10.1109/TSG.2015.2510747.

[12] G. Li, J. Liang, F. Ma, C. E. Ugalde-Loo, and H. Liang, "Analysis of single-phase-to-ground faults at the valve-side of HB-MMCs in HVDC systems," *IEEE Trans. Ind. Electron.*, vol. 66, no. 3, pp. 2444–2453, Mar. 2019, doi: 10.1109/TIE.2018.2829666.

[13] G. Li, J. Liang, T. Joseph, T. An, J. Lu, M. Szechtman, B. R. Andersen, and Q. Zhuang, "Feasibility and reliability analysis of LCC DC grids and LCC/VSC hybrid DC grids," *IEEE Access*, vol. 7, pp. 22445–22456, 2019, doi: 10.1109/ACCESS.2019.2898387.

[14] L.-Q. Liu and C.-X. Liu, "VSCs-HVDC may improve the electrical grid architecture in future world," *Renew. Sustain. Energy Rev.*, vol. 62, pp. 1162–1170, Sep. 2016, doi: 10.1016/j.rser.2016.05.037.

[15] T. An, G. Tang, and W. Wang, "Research and application on multi-terminal and DC grids based on VSC-HVDC technology in China," *High Voltage*, vol. 2, no. 1, pp. 1–10, Mar. 2017, doi: 10.1049/hve.2017.0010.

[16] A. Wu, Z. Yuan, H. Rao, B. Zhou, and H. Li, "Analysis of power transmission limit for the VSC-HVDC feeding weak grid," *J. Eng.*, vol. 2019, no. 16, pp. 2916–2920, Mar. 2019, doi: 10.1049/joe.2018.8475.

[17] K. Jia, R. Chen, Z. Xuan, Z. Yang, Y. Fang, and T. Bi, "Fault characteristics and protection adaptability analysis in VSC-HVDC-connected offshore wind farm integration system," *IET Renew. Power Gener.*, vol. 12, no. 13, pp. 1547–1554, Oct. 2018, doi: 10.1049/iet-rpg.2017.0793.

[18] I. M. Sanz, P. D. Judge, C. E. Spallarossa, B. Chaudhuri, and T. C. Green, "Dynamic overload capability of VSC HVDC interconnections for frequency support," *IEEE Trans. Energy Convers.*, vol. 32, no. 4, pp. 1544–1553, Dec. 2017, doi: 10.1109/TEC.2017.2712909.

[19] S. Kim, A. Yokoyama, Y. Takaguchi, T. Takano, K. Mori, and Y. Izui, "Small-signal stability-constrained optimal power flow analysis of multiterminal VSC-HVDC systems with large-scale wind farms," *IEEJ Trans. Electr. Electron. Eng.*, vol. 14, no. 7, pp. 1033–1046, Jul. 2019, doi: 10.1002/tee.22898.

[20] S. Sayed and A. Massoud, "Minimum transmission power loss in multi-terminal HVDC systems: A general methodology for radial and mesh networks," *Alexandria Eng. J.*, vol. 58, no. 1, pp. 115–125, Mar. 2019, doi: 10.1016/j.aej.2018.12.007.

[21] S. D. Tavakoli, E. Prieto-Araujo, E. Sánchez-Sánchez, and O. Gomis-Bellmunt, "Interaction assessment and stability analysis of the MMC-based VSC-HVDC link," *MDPI Energies J.*, vol. 13, no. 8, pp. 1–19, 2020, doi: 10.3390/en13082075.

[22] H. S. Ramadan, A. Fathy, and M. Becherif, "Optimal gain scheduling of VSC-HVDC system sliding mode control via artificial bee colony and mine blast algorithms," *IET Gener., Transmiss. Distrib.*, pp. 661–669, Sep. 2017, doi: 10.1049/iet-gtd.2017.0935.

[23] A. Raza, Z. Yousaf, M. Jamil, S. O. Gilani, G. Abbas, M. Uzair, S. Shaheen, A. Benrabah, and F. Li, "Multi-objective optimization of VSC stations in multi-terminal VSC-HVDC grids, based on PSO," *IEEE Access*, vol. 6, pp. 62995–63004, 2018, doi: 10.1109/ACCESS.2018.2875972.

[24] Y. Wang, Y. Zhou, D. Li, D. Shao, K. Cao, and K. Zhou, "The influence of VSC-HVDC reactive power control mode on AC power system stability," *MDPI Energies J.*, vol. 13, no. 7, pp. 1–11, 2020, doi: 10.3390/en13071677.

[25] R. F. Mochamad and R. Preece, "Assessing the impact of VSC-HVDC on the interdependence of power system dynamic performance in uncertain mixed AC/DC systems," *IEEE Trans. Power Syst.*, vol. 35, no. 1, pp. 63–74, Jan. 2020, doi: 10.1109/TPWRS.2019.2914318.
[26] A. Alassi, S. Bañales, O. Ellabban, G. Adam, and C. MacIver, "HVDC transmission: Technology review, market trends and future outlook," *Renew. Sustain. Energy Rev.*, vol. 112, pp. 530–554, Sep. 2019, doi: 10.1016/j.rser.2019.04.062.
[27] E. Acha, P. Roncero-Sanchez, A. V. de la Jaen, L. M. Castro, and B. Kazemtabrizi, "Power Flows," in *VSC FACTS HVDC: Analysis, Modelling and Simulation in Power Grids*. Hoboken, NJ, USA: Wiley, 2019, pp. 99–157.
[28] M. E. Montilla-djesus and D. Santos-martin, "Optimal Power Transmission of Offshore Wind Power Using a VSC-HVDC Interconnection," *MDPI Energies J.*, vol. 10, no. 7, pp. 1–16, 2017, doi: 10.3390/en10071046.
[29] Y. Li and Y. Li, "Security-constrained multi-objective optimal power flow for a hybrid AC/VSC-MTDC system with lasso-based contingency filtering," *IEEE Access*, vol. 8, pp. 6801–6811, 2020, doi: 10.1109/ACCESS.2019.2963372.
[30] B. O. Adewolu and A. K. Saha, "Performance evaluation of FACTS placement methods for available transfer capability enhancement in a deregulated power networks," in *Proc. Int. SAUPEC/RobMech/PRASA Conf.*, Jan. 2020, pp. 1–6, doi: 10.1109/SAUPEC/RobMech/PRASA48453.2020.9041146.
[31] E. Karami, G. B. Gharehpetian, H. Mohammadpour, A. Khalilinia, and A. Bali, "Generalised representation of multi-terminal VSC-HVDC systems for AC–DC power flow studies," *IET Energy Syst. Integr.*, vol. 2, no. 1, pp. 50–58, Mar. 2020, doi: 10.1049/iet-esi.2019.0051.
[32] B. O. Adewolu and A. K. Saha, "Evaluation of performance index methodology for power network contingency ranking," in *Proc. Int. SAUPEC/RobMech/PRASA Conf.*, Jan. 2020, pp. 2–7, doi: 10.1109/SAUPEC/RobMech/PRASA48453.2020.9041137.
[33] B. O. Adewolu and A. K. Saha, "FACTS devices loss consideration in placement approach for available transfer capability enhancement," *Int. J. Eng. Res. Afr.*, vol. 49, pp. 104–129, Jun. 2020, doi: 10.4028/www.scientific.net/JERA.49.104.
[34] M. Venkateswara Rao, S. Sivanagaraju, and C. V. Suresh, "Available transfer capability evaluation and enhancement using various FACTS controllers: Special focus on system security," *Ain Shams Eng. J.*, vol. 7, no. 1, pp. 191–207, Mar. 2016, doi: 10.1016/j.asej.2015.11.006.
[35] S. Burada, D. Joshi, and K. D. Mistry, "Contingency analysis of power system by using voltage and active power performance index," in *Proc. IEEE 1st Int. Conf. Power Electron., Intell. Control Energy Syst. (ICPEICES)*, Jul. 2016, pp. 1–5, doi: 10.1109/ICPEICES.2016.7853352.

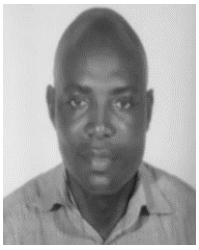

BABATUNDE OLUSEGUN ADEWOLU (Member, IEEE) received the B.Eng. degree (Hons.) (Upper Division) in electrical engineering from the University of Ilorin, Nigeria, in 2006, and the M.Sc. degree (Hons.) in electronic and electrical engineering from Obafemi Awolowo University, Ile-Ife, Nigeria, in 2012. He is currently pursuing the Ph.D. degree in electrical engineering with the University of KwaZulu-Natal, Durban, South Africa.

He has a wide industrial experience and expertise spanning a decade in the field of electrical engineering. He is a registered Engineer with the Council for the Regulation of Engineering in Nigeria, and a member of other professional bodies. His area of interests include, but not limited, to power system analysis, power system deregulation and restructuring, applications of FACTS devices, renewable energy systems, and distributed generations and integrations.

AKSHAY KUMAR SAHA (Member, IEEE) received the bachelor's degree in electrical engineering and the Ph.D. degree in electrical engineering from Jadavpur University, in 1999 and 2009, respectively. He worked at CESC Limited, a Kolkata-based Electric Power Utility, for 19 years. He is currently an Associate Professor and Academic Leader of Research and Higher Degrees at the School of Engineering, University of KwaZulu-Natal. His research interest includes advances in power systems. He is registered as a Professional Engineering with the Engineering Council of South Africa, a Fellow of South African Institute of Electrical Engineers, a Senior Member of the Society for Automation, Measurement, Instrumentation and Control, and an Individual Member of Cigré.